

# Numerical modeling of pullout tests in an extremely soft, sensitive, and thixotropic clay

Naloan C. Sampa<sup>1</sup>, Fernando Schnaid<sup>2</sup>, Marcelo M. Rocha<sup>2</sup>, Roberto Cudmani<sup>3</sup>, Claudio dos S. Amaral<sup>4</sup>

<sup>1</sup>*Dept. of Civil Engineering, Federal University of Santa Catarina  
João Pio Duarte da Silva - 205, 88040-900, Santa Catarina, Brazil  
naloan.sampa@ufsc.br*

<sup>2</sup>*Dept. of Civil Engineering, Federal University of Rio Grande do Sul  
Rio Grande do Sul, Brazil  
fschnaid@ufrgs.br, marcelo.maiarocha@gmail.com*

<sup>3</sup>*Geotechnical Center, Technical University of Munich  
Munich, Germany*

*robertocudmani@tum.de*

<sup>4</sup>*Petrobras – Petróleo Brasileiro S.A.  
amaralcs@petrobras.com.br*

**Abstract.** Three usual challenges related to numerical modeling of geotechnical problems are addressed in this paper - large distortions of finite element meshes, the soil-structure interface, and calibration of soft clay parameters. The objective of this paper is to obtain a reliable numerical model to reproduce experimental results and perform parametric analysis. The paper presents the approaches and techniques adopted to numerically simulate pullout tests of mini piles submitted to large displacements in extremely soft, sensitive, and thixotropic clay. A two-dimensional finite element model was assumed, considering the axisymmetric condition, to simulate the fluid coupled analysis in Abaqus/CAE software, taking into account two conditions: saturated clay and pullout undrained loading. Considerations and conclusions on the mobilization mechanisms of the total pullout force, base resistance and shaft resistance, and the influence of the parameters were presented and discussed. The validity of the approaches and techniques used was highlighted by the good agreement between the numerical and experimental results. The quality of the parametric results corroborates the conclusion that the numerical model is reliable and the software is a powerful tool to analyze complex interface problems related to piles embedded in very soft clay.

**Keywords:** numerical modeling, soft clay, pullout tests, large deformation, soil-structure interaction.

## 1 Introduction

Mooring lines commonly used to connect offshore platforms to anchors are subjected to large displacement on marine soil during the installation, pre-tensioning, and operation phases. The large deformation of the embedded elements in sensitive clays produces a significant decrease in the mobilized resistance after the peak. This behavior, called strain softening, is not easy to model numerically since the degradation of the soil structures depends on several factors and requires more sophisticated constitutive models. A detailed discussion about the importance of strain-softening behavior for the design of offshore foundations can be found in Zhou and Randolph (2007 [1] and 2009 [2]), Chatterjee et al. (2012) [3], Xiong et al., (2017) [4], Sun et al., (2019) [5]. Previous studies have adopted different techniques to circumvent or solve the problems found in the numerical modeling of mooring lines in soft clays. Interface and convergence problems caused by the excessive distortion of finite element meshes were analyzed and discussed by Liu and Zhao (2014) [6] and Zhao and Liu (2014 [7] and 2016 [8]). Potts and Martins (1982) [9], Masín (2005) [10], and Tan et al., (2014) [11] presented and discussed some approaches necessary to numerically model the strain-softening behavior.

Considering the challenges mentioned above, this paper uses a simplified approach to obtain a reliable numerical model to reproduce experimental results and perform a parametric study. Due to the complexity of the mooring lines' geometry, all the simulations were performed with mini piles called metallic tubes. The main results about the interaction mechanisms and the factors influencing the pullout forces are presented and discussed.

## 2 NUMERICAL METHODOLOGY

To investigate the interaction mechanism between mini-piles and soft clay, a reliable numerical model that reproduces the typical behavior of the experimental results was first calibrated. Calibration consists of adjusting soil parameters and contact properties. Once the model was calibrated, a parametric study was performed to analyze the influence of the mobilization of the base (tip) resistance on the shaft resistance.

### 2.1 Model Description

This item addresses different approaches used to obtain a reliable numerical model to reproduce experimental results. Typical results measured experimentally by Sampa (2019) [12] presented a significant reduction of the pullout force after the peak, as shown in Fig. 1. In this figure, VFC, d, L, and AMT mean vertical free chain, nominal diameter, length, and sample, respectively.

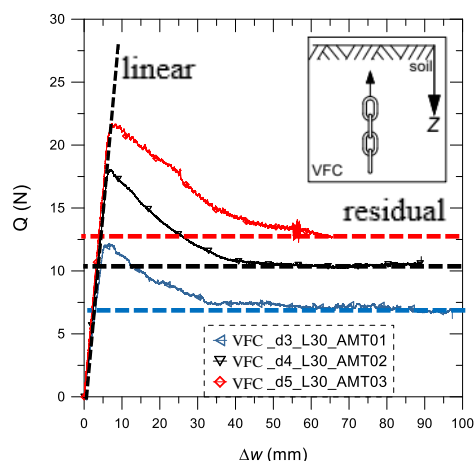
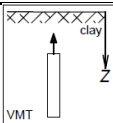
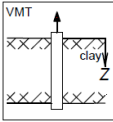


Figure 1. Typical load-displacement curves.

Two challenge problems arose during the numerical simulation of the experimental tests. The first is the convergence problem due to the large distortions of the finite element meshes. The second is the inability of the Modified Clay Cam model available at ABAQUS to model the strain-softening behavior related to the degradation of clay structures. As a result, more sophisticated models are needed to simulate this behavior, such as that used by Masín (2005) [10]. To circumvent these problems, the numerical simulation of the experimental tests was divided into two parts as shown in Tab. 1. In this table, VMT refers to the vertical metallic tube.

Table 1. Friction coefficients used in the 1<sup>st</sup> and 2<sup>nd</sup> parts.

		L=10cm	L=30cm	L=50cm	Maximum displacement (mm)
	1 <sup>st</sup> part	1,00	1,32	2,00	5
	2 <sup>nd</sup> part	0,37	0,46	0,6	100

The first part reproduced the linear section related to the small displacement ( $w$ ). Metallic tubes were modeled considering the full embedment into the soil and then pulled vertically up to 5mm necessary to mobilize the total pullout force. To reproduce the residual condition associated with the large displacement – the second part, tubes with ends off the soil were pulled vertically up to 100mm, considering only the shaft resistance. In both conditions, three tubes with an external diameter of 25 mm and lengths of 10, 30, and 50 cm were considered.

A two-dimensional finite element model was created to simulate the fluid coupled analysis, taking into account saturated clay and undrained loading condition. The soil domain was modeled as an elastoplastic material obeying the Modified Cam Clay yield criterion, while the tubes were modeled as rigid bodies with isotropic linear elastic behavior, obeying the Mohr-Coulomb failure criterion. The soil properties were determined from a mix of 85% of kaolin and 15% of sodium bentonite that has been used by Sampa (2019) [12]. The main properties of the materials are summarized in Tab. 2.

Table 2. Material properties.

Soft clay	Parameters	$\kappa$	$\nu$	$\Lambda$	$M$	$a_0$	$e_0$	$\rho_d$	$k$ (m/day)
	Values	0,08	0.3	0,46	0.8	3,1	3,9	0,63	4,96E-5
Metallic mini-piles	Parameters	$E$ (kN/m <sup>3</sup> )	$\nu$	$P$					
	Values	2.1e8	0.285	0,91					

The domain size of the numerical model was similar to that of the experimental tests – radius = 12cm and length = 72cm. Due to the symmetry, only half of the domain was modeled, as shown in Fig. 2. The bottom horizontal boundary is restricted in both the axial (vertical) and radial (horizontal) directions. The vertical boundary is restricted only along the radial direction. The boundary condition in the central line is considered axisymmetric in the radial direction, while the top horizontal boundary is considered permeable.

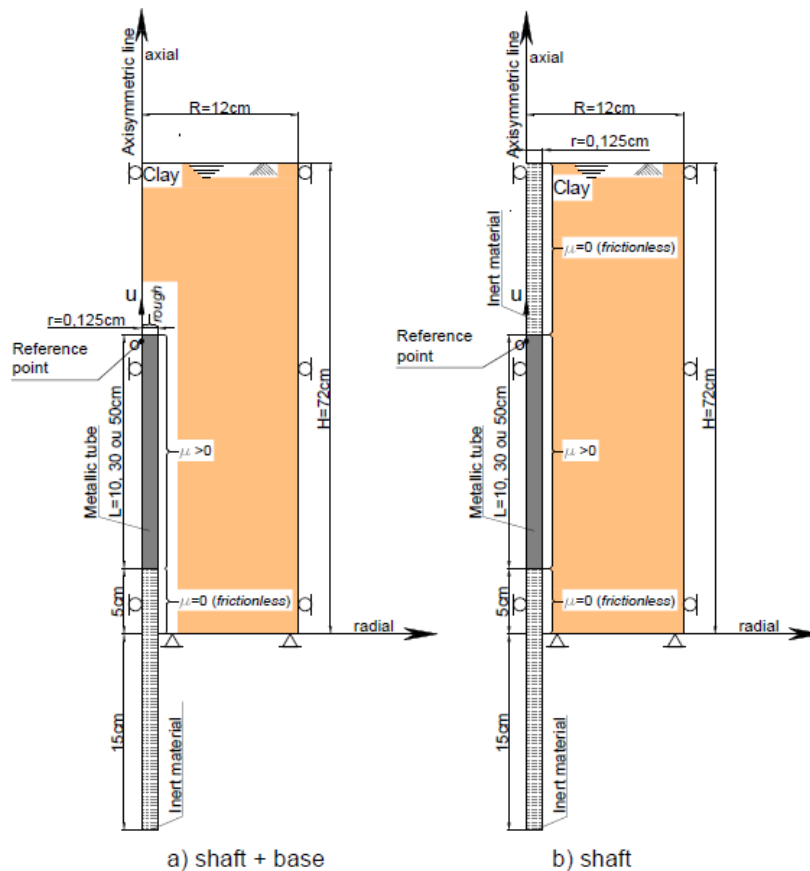


Figure 2. Representation of the domain size of the numerical model a) fully embedded tube b) tube with ends off the soil.

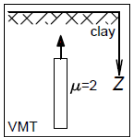
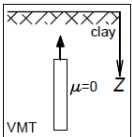
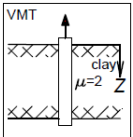
For both materials, an axisymmetric mesh with quadrilateral elements has been used. Element types of CAX8R and CAX8RP were used to model metallic tubes and clay soil, respectively. Finer meshes in the soil domain were considered near the tube due to higher concentrations of stresses and deformations in these regions. The contact surfaces between the metallic tube and the soil were discretized using the surface-to-surface contact technique with the master-slave contact algorithm. The contact properties in the normal direction were implemented using the direct method called hard contact. Coulomb's contact formulation was used to represent the tangential behavior at the soil-tube interface. The shear stress ( $\tau$ ) between the contact surfaces was calculated by the expression  $\tau = \mu \cdot \sigma$ , where  $\sigma$  is the normal contact pressure and  $\mu$  is the friction coefficient. The values of the friction coefficient are shown in Tab. 1. For fully embedded tubes, the interaction between the upper end and the soil was considered rough, with no possibility of sliding. For tubes with ends off the soil, their surplus lengths were modeled as an inert material, weightless and frictionless with soil.

The numerical simulation was performed in four steps, according to the sequence of the experimental tests. The first step was to generate initial geostatic stresses using the Body Force option. The metallic tube was installed in the second step using the replacement technique. In the third step, the consolidation process by its weight was simulated for a period of 24-hour. In this step, the top horizontal boundary of the soil was considered permeable. In the fourth step, the tube was subjected to a vertical increasing displacement-controlled load ( $u$ ) of 5mm/s at the reference point, as shown in Fig. 2.

### 2.2 Parametric Analysis

Once the numerical model was calibrated, a parametric study was carried out to investigate the interaction mechanisms and analyze the influence of the mobilization of the base (tip) resistance on the shaft resistance. Unlike piles subjected to compression, the mobilization of the base resistance of fully embedded tubes subjected to tension begins at the initial moment of the displacement. As a consequence of this mechanism, the shaft resistance is strongly affected. To investigate all these mechanisms, three cases – A, B, and C – were modeled with tubes of different diameters and lengths. Case A simulates a fully embedded tube, considering both the base and the shaft resistances. Case B also simulates a fully embedded tube but considers only the base resistance. This case provides a better understanding of the influence of the mobilization of the base (tip) resistance on the shaft resistance. Case C simulates a metallic tube with ends off the soil taking into account only the shaft resistance. The soil model calibrated before was used in all cases of the parametric study. Table 3 presents the values of diameter, length, and friction coefficients of all cases. In this table, VMT means the vertical metallic tube.

Table 3. Three cases analyzed in the parametric study.

	Case A	Case B	Case C
			
Diameter (mm)	25, 27 e 29	25, 27 E 29	25, 27 E 29
Length (cm)	10, 20 e 50	10, 20 e 50	10, 20 e 50
Shaft resistance ( $\mu$ )	yes (2,0)	no (0)	yes (2,0)
Base resistance	Yes	Yes	No
Ends of the tube	embedded	embedded	not embedded

### 3 Results and Discussion

Figure 3(a)–(c) show a comparison between experimental and numerical results related to the fully embedded tubes with 10, 30, and 50cm in length, respectively.  $Q$ ,  $q_s$ ,  $q_b$ ,  $W$  and  $w/D$  mean total pullout force, shaft resistance, base resistance, tube's weight, and normalized displacement, respectively.  $Q$  is the sum of the  $q_b$ ,  $q_s$  and  $W$ . For experimental results, the maximum values of  $q_s$  and  $q_b$  were estimated from the total pullout force and are represented by a point, since only the total pullout force was measured experimentally.

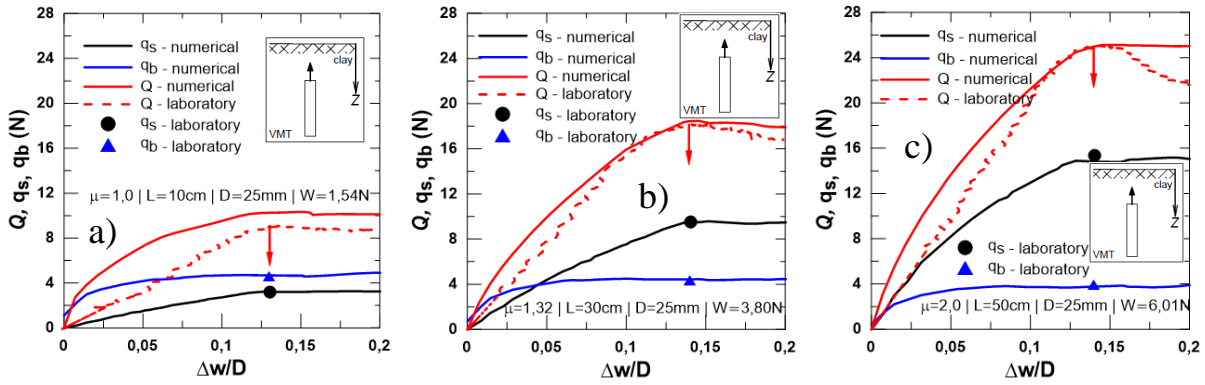


Figure 3. embedded tubes - Comparison between curves of laboratory and numerical investigations - a) 10 cm long tube; b) 30 cm long tube; c) 50 cm long tube.

A good agreement between the experimental and numerical results can be seen in Fig. 3, indicating the reliability of the numerical model. The influence of the base resistance on the total pullout force decreases as the tube length increases. The  $q_b$  curve from the numerical simulation shows the mobilization of the base resistance before the complete mobilization of the lateral resistance. This behavior is discussed in more detail in the parametric study item.

Figure 4(a)–(c) compares the lateral resistances calculated from numerical simulation and experimental tests. A good agreement can again be observed between the experimental and numerical results. Based on the calibration results, it is possible to conclude that the numerical model is reliable and presents satisfactory results from a practical point of view and, therefore, it can be used in the parametric study.

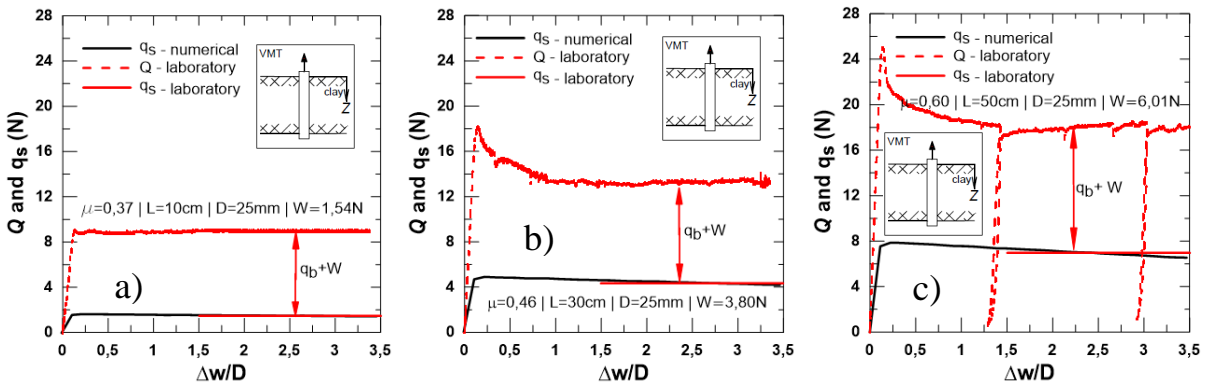


Figure 4. not embedded tubes - Comparison between curves of laboratory and numerical investigations - a) 10 cm long tube; b) 30 cm long tube; c) 50 cm long tube.

Regarding the parametric study, a total of three cases was numerically modeled and their results are shown in Figs. 5, 6, and 7, corresponding to the lengths of 10, 30, and 50 cm, respectively. These figures present three curves for case A - total pullout force, base resistance, and shaft resistance. Besides, the base resistance and shaft resistance curves for cases B and C, respectively, are also shown in these figures.

As expected, the results show an increase in the total pullout force with increasing diameter, length, and undrained shear strength. A trend towards the linearization of the initial section of the curve of the total pullout force can be observed as the length of the tube increases. This behavior is not dependent on the diameter of the tube.

A good agreement can be observed between the curves of cases A and B, regardless of the diameter and length of the tube. This observation corroborates the conclusion that the mobilization process of the shaft resistance does not influence the magnitude of the base resistance. As explained previously, the mobilization process of the base resistance starts as soon as the tube is displaced, not depending on the subsequent mobilization of the shaft resistance. The soil in front of the tube is compressed and dragged upwards by the upper end of the tube. For small displacements,  $\Delta w / D < 2.5\%$ , the base resistance is greater than the shaft resistance.

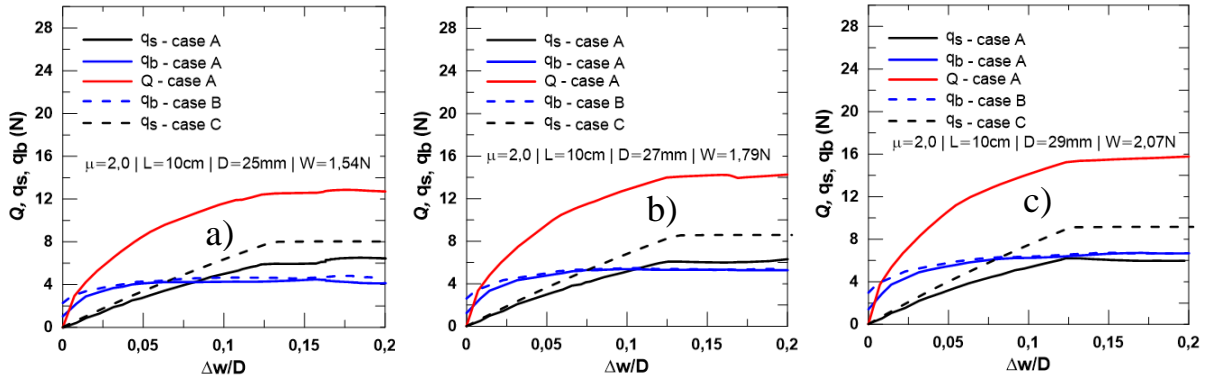


Figure 5. Load  $\times$  normalized displacement curves of cases A, B, and C - a) 10cm long tube and 25mm in diameter; b) 10cm long tube and 27mm in diameter; c) 10cm long tube and 29mm in diameter.

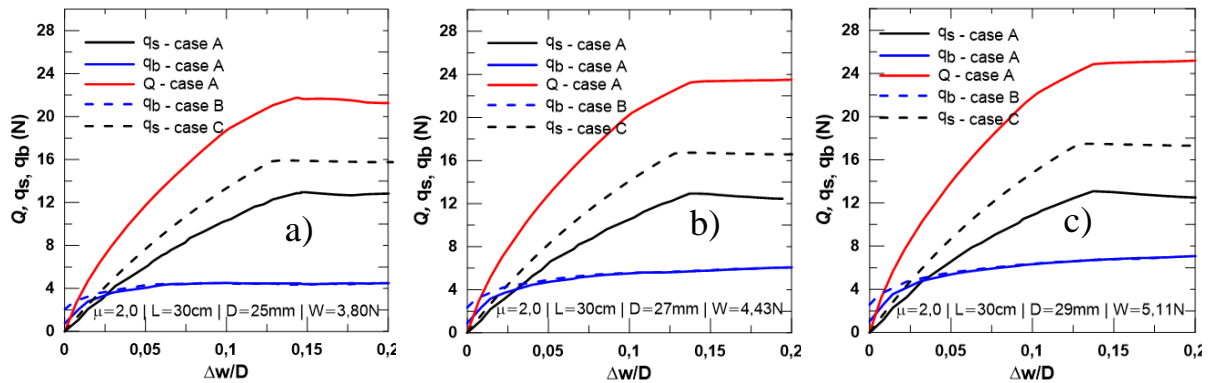


Figure 6. Load  $\times$  normalized displacement curves of cases A, B, and C - a) 30cm long tube and 25mm in diameter; b) 30cm long tube and 27mm in diameter; c) 30cm long tube and 29mm in diameter.

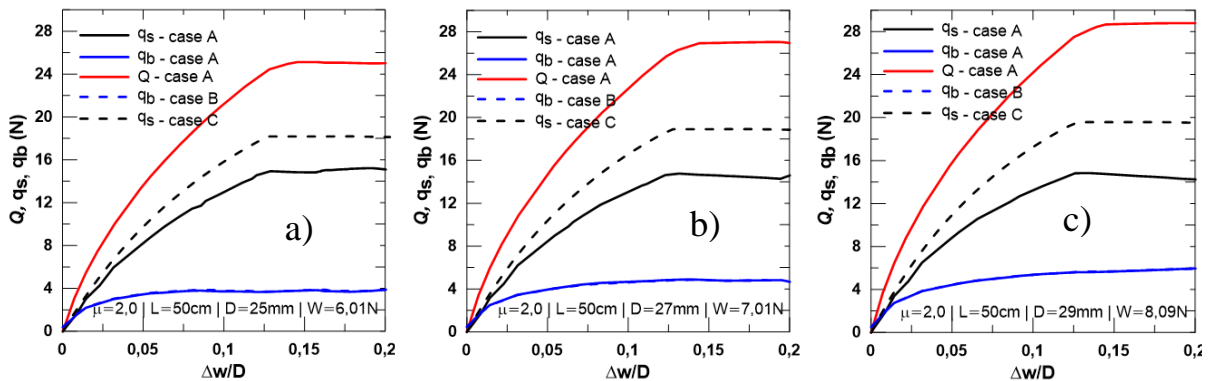


Figure 7. Load  $\times$  normalized displacement curves of cases A, B, and C - a) 50cm long tube and 25mm in diameter; b) 50cm long tube and 27mm in diameter; c) 50cm long tube and 29mm in diameter.

A direct comparison between the shaft resistances of cases A and C clearly shows higher values for case C, regardless of the size of the tubes and the displacement submitted. Larger reductions of the shaft resistance in case A are observed in larger diameters and shorter lengths. For 10 cm long tubes, the ratios between the shaft resistances of cases A and C are 81.7% (D=25mm), 73.3% (D=27mm), and 67.4% (D=29mm). For 30 cm long tubes, the ratios between the shaft resistances of cases A and C are 81.3% (D=25mm), 77.3% (D=27mm), and 74.94% (D=29mm). For 50 cm long tubes, the ratios between the shaft resistances of cases A and C are 83.5% (D=25mm), 78.1% (D=27mm), and 75.5% (D=29mm). These results lead to the conclusion that the shaft resistance of fully embedded tubes subjected to tension should always be considered less than the shaft resistance of tubes with ends off the soil. The average values of the adhesion factors ( $\alpha$ ) measured in the numerical simulation for case A present in the same order of magnitude of those estimated experimentally (0.35 – 0.50) taking into account the variation of the undrained shear strength with the depth. As a consequence of the



embedment, the adhesion factors of case A are always lower than those for case C.

## 4 Conclusions

This paper investigated through numerical simulation the interaction mechanisms between metallic mini piles and soft clays. Different approaches were used to overcome three usual challenges related to numerical modeling of geotechnical problems - large distortions of finite element meshes, the soil-structure interface, and calibration of soft clay parameters. The numerical model calibrated based on high-quality laboratory results seems reliable and presents satisfactory results from a practical point of view.

The results of the numerical modeling indicate that the base resistance is fully mobilized before the complete mobilization of the shaft resistance. Due to the embedment of the tubes, the mobilization process of the base resistance starts as soon as the tube is displaced, and its performance is not affected by the subsequent mobilization of the shaft resistance. On the other hand, the shaft resistance is strongly affected by the mobilization process of the base resistance. For offshore foundation in soft clay, the shaft resistance of fully embedded elements (mooring lines and piles) subjected to large deformation during tensioning must always be considered less than the shaft resistance of the same element with ends off the soil or subjected to compression.

Some improvements can be made as a continuation of this study – 1) to capture the strain-softening behavior of the thixotropic and sensitive soft clay, a more sophisticated constitutive model needs to be implemented in ABAQUS; b) the Arbitrary Lagrangian-Eulerian approach should be used to model problems of offshore foundations subjected to large deformations.

**Acknowledgments.** The authors wish to express their gratitude to the Federal University of Rio Grande do Sul and the Technical University of Munich for the infrastructure and, to CNPq, CAPES, and Petrobras for the financial support during the research project.

**Authorship statement.** The authors hereby confirm that they are the sole liable persons responsible for the authorship of this work and that all material that has been herein included as part of the present paper is either the property (and authorship) of the authors or has the permission of the owners to be included here.

## References

- [1] H. Zhou and M. F. Randolph. “Computational Techniques and Shear Band Development for Cylindrical and Spherical Penetrometers in Strain-Softening Clay”. *International Journal of Geomechanics*, vol. 7, n. 4, pp. 287–295, 2007.
- [2] H. Zhou and M. F. Randolph. “Resistance of full-flow penetrometers in rate-dependent and strain-softening clay”. *Géotechnique*, vol. 59, n. 2, pp. 79–86, 2009.
- [3] S. Chatterjee; M. F. Randolph; D. J. White. “The effects of penetration rate and strain softening on the vertical penetration resistance of seabed pipelines”. *Géotechnique*. vol. 62, n. 7, pp. 573–582, 2012.
- [4] L. Xiong; D. J. White; S. R. Neubecker; W. Zhao and J. Yang. “Anchor loads in taut moorings: The impact of inverse catenary shakedown”. *Applied Ocean Research*, vol. 67, pp. 225–235, 2017.
- [5] C. Sun; X. Feng; S. R. Neubecker; M. F. Randolph; M. F. Bransby and S. Gourvenec. “Numerical Study of Mobilized Friction along Embedded Catenary Mooring Chains”. *Geotech. Geoenviron. Eng.*, vol. 145, pp. 1–13, 2019.
- [6] H. Liu and Y. Zhao. “Numerical study of the penetration mechanism and kinematic behavior of drag anchors using a coupled Eulerian-Lagrangian approach”. *Geotechnical Engineering Journal of the SEAGS & AGSSEA*, vol. 45, pp. 29–39, 2014.
- [7] Y. Zhao and H. Liu. “Numerical simulation of drag anchor installation by a large deformation finite element technique”. In: 33rd International Conference on Ocean, Offshore, and Arctic Engineering, Proceedings...pp. 8 -13. jun. 2014.
- [8] Y. Zhao and H. Liu. “Numerical implementation of the installation/mooring line and application to analyzing comprehensive anchor behaviors”. *Applied Ocean Research*, vol. 54, pp. 101–114, 2016.
- [9] D. M. Potts and J. P. Martins. “The shaft resistance of axially loaded piles in clay”. *Géotechnique*, vol. 32. n. 4. pp. 369–386, 1982.
- [10] D. Masín. “A hypoplastic constitutive model for clays”. *International Journal for Numerical and Analytical Methods in Geomechanics*, vol. 29, n. 4, pp. 331 – 336, 2005.
- [11] S. A. Tan, J. Sun, K. S. Ng. “Numerical simulation of strain softening behavior at pile- soil interface”. In: 8th European Proceedings ..., Conference on Numerical Methods in Geotechnical Engineering, Delft, June, 2014.
- [12] N. C. Sampa. Modeling of the Interaction Mechanisms of Offshore Platforms Mooring Lines in Clay Soils. 2019, PhD thesis, Federal University of Rio Grande do Sul, Brazil, 2019.